Molecular Crystals and Liquid Crystals

Publication details, including instructions for authors and subscription information:
http://www.tandfonline.com/loi/gmcl20

Diffuse Scattering from Organic Crystals

T. R. Welberry [a]

[a] Research School of Chemistry, The Australian National University, Canberra, ACT, Australia

Version of record first published: 31 Aug 2006

To cite this article: T. R. Welberry (2005): Diffuse Scattering from Organic Crystals, Molecular Crystals and Liquid Crystals, 440:1, 1-21

To link to this article: http://dx.doi.org/10.1080/15421400590957576

Mol. Cryst. Liq. Cryst., Vol. 440, pp. 1–21, 2005

ISSN: 1542-1406 print/1563-5287 online
DOI: 10.1080/15421400590957576

Taylor & Francis
Taylor & Francis Group

Diffuse Scattering from Organic Crystals

T. R. Welberry
Research School of Chemistry, The Australian National University, Canberra, ACT, Australia

The measurement of diffuse scattering data over large volumes of reciprocal space is now relatively routine and this opens up the possibility of analysing the local atomic and molecular structure of crystals in a level of detail not possible via conventional crystallography. We describe the development of a general method by which such diffuse scattering data can be analysed. This involves Monte Carlo simulation of a model crystal from which diffraction patterns may be calculated and compared to the observed data. The method is illustrated using two contrasting organic molecular crystal examples. For benzil, $C_{14}H_{10}O_2$, the diffuse scattering is purely thermal in origin while ClMe (p–methyl–N-(p-chlorobenzylidene) aniline, $C_{14}H_{12}ClN$) is very disordered with each molecular site being occupied by the molecule in one of four different basic orientations and considerable local relaxation of these basic positions and orientations is present.

Keywords: benzil; diffuse scattering; disordered crystals; Monte Carlo simulation; *p*-methyl-*N*-(*p*-chlorobenzylidene)aniline

1. INTRODUCTION

Conventional crystal structure analysis using Bragg diffraction data reveals only average one-body structural information, such as atomic positions, thermal ellipsoids and site occupancies. Diffuse scattering, on the other hand, gives two-body information and is thus potentially a rich source of information on how atoms and molecules interact with each other. That diffuse scattering intensities are typically several orders of magnitude lower than for the Bragg peaks has meant that such information has frequently been ignored. However modern developments in X-ray sources (synchrotrons) and detectors (linear-detectors,

Financial support of the Australian Research Council and the Access to Major Research Facilities Program is gratefully acknowledged.

Address correspondence to T. R. Welberry, Research School of Chemistry, The Australian National University, Canberra, ACT 0200, Australia. E-mail: welberry@rsc.anu.edu.au

area-detectors, image plates) and even developments in neutron diffraction have enormously increased the capability for measuring such weak data and this aspect of the field of study, though still presenting challenges, is no longer a limiting factor.

The greater challenges occur in the interpretation and analysis of diffuse scattering. Traditional approaches, developed largely in the field of alloys and simple oxides [1,2], present insurmountable difficulties when systems become more complex or when the magnitudes of atomic displacements become relatively large [3]. Considerable progress has been made in an alternative approach to understanding the local atomic and molecular arrangements and interactions in disordered crystals, which overcomes some of these difficulties [4]. The method consists of comparing diffraction patterns calculated from a computer model (usually Monte Carlo simulation) of the disordered structure with measured (X-ray) diffuse intensities.

We have reported investigations of a wide variety of disordered crystals in which we have used Monte Carlo (MC) simulation to aid in the interpretation and subsequently to analyse observed diffuse X-ray scattering patterns [5–11]. The general approach is to set up a computer model of the disordered structure using sets of random variables to represent the atomic occupancies and positions or molecular orientations. A relatively small number of energy parameters are used to describe the way in which these atoms or molecules interact. MC simulation is then carried out for a time sufficient to allow the system to approach equilibrium. The final atomic coordinates of this model crystal realisation are then used to calculate diffraction patterns, which are then compared to the observed X-ray patterns. After assessing the points of agreement and disagreement from this comparison the model parameters are adjusted and the whole process is repeated iteratively until a satisfactory agreement between observed and calculated patterns is obtained. Initially, this fitting process was performed by trial and error [7] but more recently a least-squares (LS) fitting procedure has been developed [12] which promises to place the modeling process on a much more quantitative footing. This LS procedure is very computer intensive, but with the advent of ever faster and cheaper computers it is increasingly becoming feasible to tackle ever more complex systems.

The advantage of the MC methodology is that it can be applied generally to all systems regardless of their complexity or the size of the atomic displacements that might be present. If a model derived in this way gives a calculated diffraction pattern that agrees with observation then considerable confidence can be attached to the model since it is based on plausible physical and/or chemical principles. On the other hand models which do not so agree can readily be rejected.

In this paper we describe two contrasting examples to illustrate the level of detail that can currently be achieved. The two systems we describe here are the molecular crystals benzil, $C_{14}H_{10}O_2$ [13], and *p*-methyl-*N*-(*p*-chlorobenzylidene) aniline, $C_{14}H_{12}ClN$, (ClMe) [14].

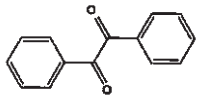

Benzil

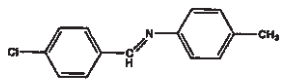

ClMe

Study of these two compounds is part of a long-term project in which we investigate the effect of internal molecular flexibility on the structure and stability of crystals. In each case the molecules have internal torsion angles which are expected to allow low energy motions or conformation changes. However, while benzil forms an ordered structure with all molecular sites occupied by the molecule in essentially the same orientation, ClMe forms a very disordered structure in which each molecular site is occupied by the molecule in one of four different basic orientations. These two systems therefore present quite different challenges to the current methodology.

In the sections that follow we first describe the experimental measurement of the diffuse scattering data using a conventional laboratory X-ray source. In addition we refer to developments in which data may be obtained using synchrotron radiation or even using neutrons from a spallation source. We then describe the setting up of Monte Carlo simulations to model the two example compounds, showing how in each case the problem is formulated in terms of a limited number of adjustable parameters. We then briefly review the least-squares fitting method using the benzil example to illustrate various concepts. Finally we show the results for the two compounds and discuss the implications of the derived structural parameters.

2. MEASUREMENT OF DIFFUSE SCATTERING

The diffuse scattering data used for the study of the two example compounds was obtained using the position-sensitive diffractometer system shown in Figure 1. The apparatus utilizes the so-called flat-cone geometry and has been described in detail elsewhere [15]. It comprises the following key features. X–rays are produced by a conventional X-ray tube (most often using a Cu target). A graphite monochromator is used to select the characteristic (e.g. CuKα) radiation which is then passed down a collimator tube aligned to deliver the X-rays through the centre of rotation of a 3-axis goniometer. The length of the collimator

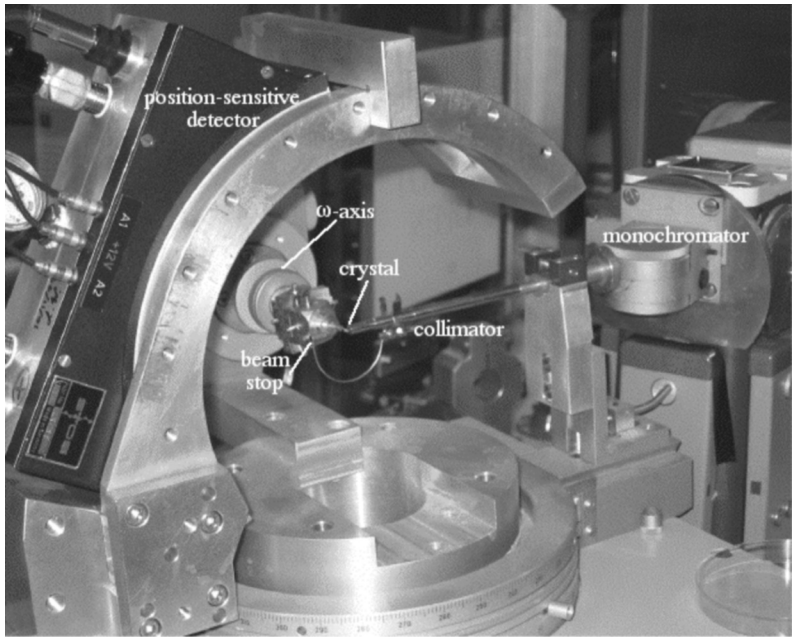

FIGURE 1 Position-sensitive detector diffractometer for collecting diffuse scattering data on a conventional laboratory source.

is such that the exit aperture (of ~ 0.5 mm diameter) is only about 1 mm from the sample crystal. This arrangement is crucial in keeping air-scattering to a minimum, as is the placement of a beam stop close behind the sample. The crystal is prealigned about an horizontal rotation axis ω. The curved position-sensitive wire detector (PSD) records X-rays scattered by the sample. X-rays scattered over a range of diffraction angle up to $2\theta = \sim 51^\circ$ are recorded with a single setting of the PSD. Data is collected as a series of stationary PSD scans as ω is incremented sequentially. Typically 1000 individual scans at 0.36° intervals are used to provide a complete sweep through a single section of the diffraction pattern. In the configuration shown, the plane containing both the incident and diffracted X-rays recorded by the detector is normal to the rotation axis. This provides data in the zero-level section of the diffraction pattern for the particular rotation axis, ω.

In Figure 2 we show a typical diffuse scattering pattern recorded on the instrument. Figure 2a shows the raw data displayed as a 2D plot measuring 512×900 pixels. Each vertical line is a single PSD scan corresponding to 2θ and the horizontal axis corresponds to the crystal

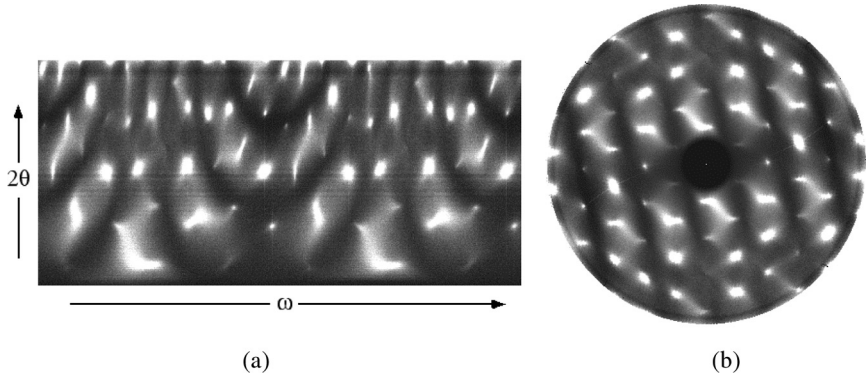

FIGURE 2 Typical diffuse scattering data obtained using the PSD diffractometer shown in Figure 1 on a laboratory source. (a) Raw data. (b) Undistorted reciprocal lattice section derived from (a).

orientation ω. Figure 2b shows the same data after transformation to reciprocal lattice coordinates. To obtain upper-level sections the two horizontal goniometer circles are rotated through an angle, μ, thus keeping the plane of the detector normal to the rotation axis, but inclining the latter away from the normal to the incident X-rays.

The resolution of the instrument is such that individual pixels in Figure 2a are essentially independent measurements. This means that the PSD provides an enhancement factor of $\sim$512 compared to a single point detector of the same resolution. Even so typical data collection times are $\sim$2–5 minutes per PSD scan or between 1–3 days per reciprocal section. Crystal dimensions of $\sim 0.5 \times 0.5 \times 0.5$ mm are optimal for this system. Synchrotron radiation offers the possibility of obtaining diffuse scattering data of better quality (lower signal to noise) in much less time and from possibly much smaller samples. Two different approaches have been reported. Experiments in which single sections of data have been recorded in an analogous manner to those described above have been reported [16]. However this type of experiment is very wasteful of the incident X-ray photons since only a very small fraction of the scattered X-rays are actually measured. Weber et al. [17] and Campbell et al. [18] have therefore used an alternative approach to record virtually complete 3D sets of diffuse scattering. In their experiments the scattered intensity for a given crystal orientation is recorded on a 2D detector – either an image plate or a CCD detector. Then, by incrementing the crystal orientation and recording many such 2D images, a full 3D data set is recorded. This may be achieved in a time comparable to that required for a single section by the earlier

method. If plane sections of data are required these can be extracted subsequently from the 3D data, although given the large quantities of data involved this is itself a not inconsiderable task.

Until recently it might have been supposed that measurement of diffuse neutron scattering over large volumes of diffraction space was not a viable proposition simply because of the much lower fluxes of neutron sources compared to X-ray sources. However with the use of the latest multi-detector arrays at modern neutron facilities it is now feasible to obtain such scattering, though much larger samples than would be used for X-rays are still required. One such system is the SXD single crystal beam-line at the ISIS pulsed neutron facility [19]. On this instrument eleven 2D detector arrays, each of which comprises 64×64 individual pixels, surround the sample, as shown in Figure 3a. The detectors subtend a substantial fraction of the total solid scattering angle. Moreover each individual pixel records a complete time-of-flight spectrum so that for any setting of the crystal an enormous quantity of data is recorded simultaneously, compensating to no small extent for the lack of flux. Figure 3b shows a 2D section from the 3D neutron pattern recorded on this facility for the molecular crystal D-benzil, $C_{14}D_{10}O_2$, using a crystal of dimensions $\sim 3 \times 6 \times 12$ mm [20]. The total counting time for this experiment was ~ 3 days. Of particular note in this diffraction pattern is the presence of diffuse scattering well beyond the Q values where Bragg peaks are observed. This is easily observable because

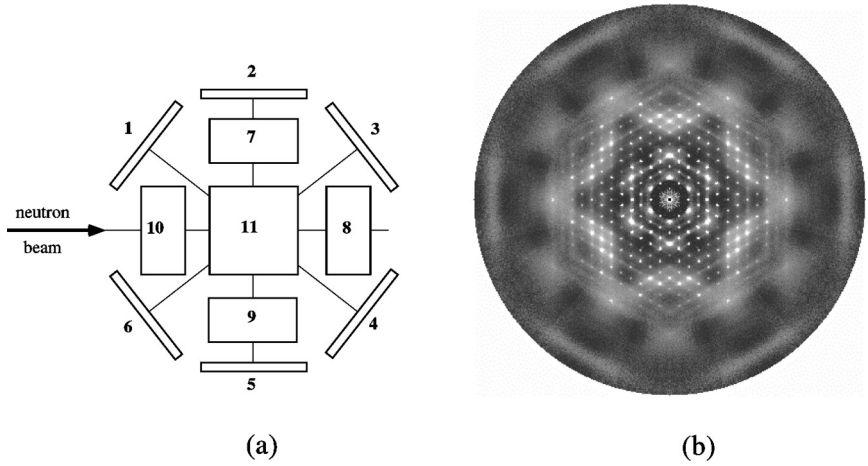

FIGURE 3 Diffuse neutron scattering. (a) Arrangement of the detectors around the sample on the SXD beamline at ISIS. (b) Diffuse neutron scattering pattern of d-benzil, $C_{14}D_{10}O_2$.

of the fact that neutron scattering lengths do not fall away at high Q in the way that X-ray scattering factors do.

3. MONTE CARLO SIMULATION

General

Semi-empirical atom-atom potential methods are widely used to model ordered molecular crystals and have reached a level of accuracy and sophistication that they may even be used to predict the crystal structures of compounds for which no X-ray structure determination is available [21]. However, for use in the MC simulation of disordered structures in which we use model crystals comprising typically $\sim 32 \times 32 \times 32$ unit cells each containing a number of different molecules, such methods are far too time consuming. Our aim when setting up a MC simulation is to replace the large number of individual atom-atom interactions with a much smaller number of 'effective' interactions that are nevertheless sufficient to define the mutual spacing and orientation of neighbouring pairs of rigid molecules or molecular fragments. These effective interactions may be chosen to link particular pairs of real atoms within different molecular fragments or alternatively may be between dummy atoms chosen to conveniently define the mutual separation and orientation of the particular fragments. The effective interactions used are in the form of harmonic (Hooke's law) springs.

$$E_s = \sum_{n,m} K_{n,m}[d_{n,m} - d_{ave}]^2 \tag{1}$$

where $\boldsymbol{d}_{n,m}$ is the instantaneous length of the spring connecting the 'atoms' n and m and $\boldsymbol{d}_{ave}$ is the length of the corresponding vector in the average crystal structure. $K_{n,m}$ are spring constants which are the system parameters that are to be determined in the analysis.

For the case of benzil, in which only one molecular orientation occurs in each average site position, equation (1) is all that is required to perform the MC simulation. However, this does not take into account the energy involved in the internal rotations of the three internal torsion angles, ϕ_1, ϕ_2, ϕ_3, shown in Figure 4a, and additional torsional spring constants, $L_{n,m}$, are defined.

$$E_t = \sum_{n,m} L_{n,m}[\phi_{n,m} - \phi_{ave}]^2 \tag{2}$$

For the case of ClMe the situation is much more complex because of the fact that a given molecular site has one of four basically different

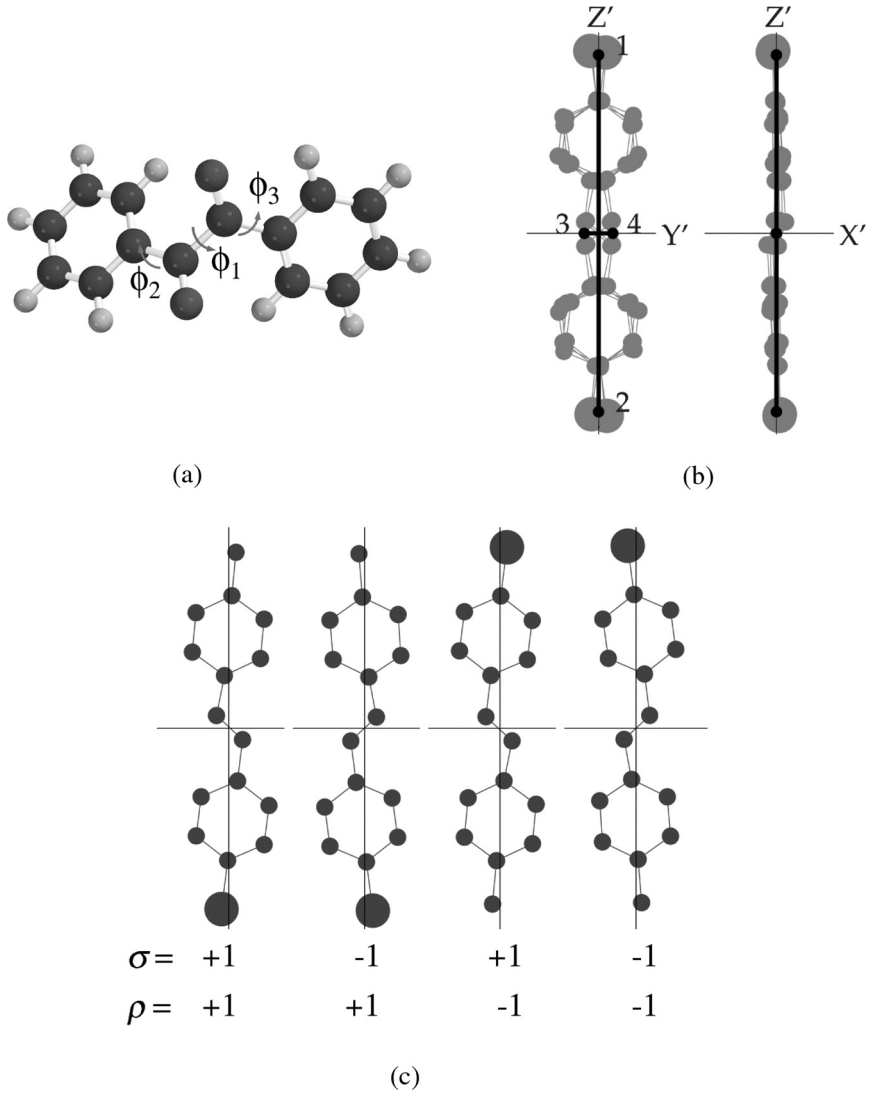

FIGURE 4 (a) The three torsion angles in benzil. (b) The 4-atom *motif* used to represent the molecule in the MC simulation ClMe. (c) The four different orientations of the ClMe molecule and the values of the random variables used to represent them.

molecular orientations present. In view of this complexity a number of simplifying approximations need to be made. First it is assumed that the whole molecule may be treated as a single rigid group and in

performing the MC simulation a *motif* comprising 4 dummy atoms is used to define the centre of mass and orientation of each molecule (see Fig. 4b). The atomic coordinates for the four different molecular orientations may be regenerated from this 4 atom *motif* after the MC simulation is complete. Now the equation (1) is no longer satisfactory because the length of the springs joining different pairs of dummy atoms might be expected to depend on which of the four molecular orientations are occupying the two linked molecular sites. Consequently equation (1) is generalised to

$$E_s = \sum_{n,m} K_{n,m}[d_{n,m} - d_{ave}(1 + \varepsilon_{n,m})]^2 \tag{3}$$

where $\varepsilon_{n,m}$ are size-effect parameters that depend on the particular pair of molecular orientations at sites n and m. The $\varepsilon_{n,m}$ provide that some interatomic distances are longer than the average while others are smaller. Since each site contains one of 4 different molecular orientations this means that there are 16 different possible values of $\varepsilon_{n,m}$ required for each different interaction vector (though there will be some constraints required to ensure the average is maintained). It is not feasible to attempt to determine such a large number of parameters and it is necessary to make further simplifications. The simplifications actually adopted are discussed later.

Equation (3) provides the MC simulation with the means to allow the molecular positions and orientations in ClMe to relax locally given the distribution of basic molecular orientations that are present. The MC model also needs to provide the means by which the basic occupancy distributions can be determined. The basic molecular orientations are represented in the computer by occupational random variables, $\sigma_{i,j,k,l}$, $\rho_{i,j,k,l}$. Here i,j,k specify the unit cell and l the particular molecular site within the unit cell. The two different occupancy variables are used to describe the end-to-end flipping of the molecule and the side-to-side flipping (see Fig. 4c). The MC energies used to specify local ordering of these molecular orientations are then in the form of Ising models:

$$E_{\mathrm{ss}} = \sum_n a_n \sigma_{i,j,k,l}\, \sigma_{i_n,j_n,k_n,l_n} \tag{4}$$

$$E_{\mathrm{ee}} = \sum_n b_n \rho_{i,j,k,l}\, \rho_{i_n,j_n,k_n,l_n} \tag{5}$$

$$E_{\mathrm{se}} = \sum_n c_n \sigma_{i,j,k,l}\, \rho_{i_n,j_n,k_n,l_n} \tag{6}$$

E_{ss} controls the correlation between the side-to-side flipping of neighbouring molecules, E_{ee} controls the correlation between the end-to-end

flipping and E_{se} allows the possibility of cross-correlation between the two types of molecular flip. Here the summations are over all $n$types of neighbour of a particular site, i,j,k,l. The a_n, b_n, c_n, are interaction parameters which govern whether particular neighbouring molecular orientations are correlated. One such set of three parameters is required for each symmetry-independent intermolecular vector along which significant correlation might be expected to occur.

In principle the MC simulation should be performed using Eqs. (3) and (4)–(6) simultaneously. This is not viable in practice, however, since any changes to the occupancy distributions occurring as a result of equation (4)–(6) will require many iterations using equation (3) to allow the new configuration to attain an energy minimum. The MC simulation is therefore carried out in two stages. The first stage uses equation (4)–(6) to determine the occupancy distribution and the second stage uses equation (3) to allow local relaxation of positions and orientations.

Benzil Simulation

Figure 5a shows a drawing of the average structure of benzil viewed down the **c** axis. The structure is seen to consist of three molecular layers which are shown in different shades of grey. Each molecule is in contact with 15 neighbouring molecules. With each molecule in its equilibrium position all intermolecular atom-atom contact distances less than 4.5 Å were computed. A smaller number of contact vectors to be used in defining the effective interactions was obtained by pruning this list. Each intermolecular contact was represented by a small number of atom-atom contacts (2 to 3) which were sufficient to define the equilibrium separation and mutual orientation of neighbouring molecular fragments. These contact vectors are also shown in Figure 5a. Around each molecule there are 34 such vectors which comprise 10 symmetry-inequivalent vector types. At a later stage, 4 additional contact vectors (1 additional vector type) were added, making a total of 11 different spring constants to be determined. A single torsional force constant was used and was assumed to apply to all three torsion angles, ϕ_1, ϕ_2, ϕ_3. One final parameter was added to the model in the form of an overall iso-tropic Debye-Waller factor, B. The MC simulation for benzil thus had a total of 13 adjustable parameters.

ClMe Simulation

Figure 5b shows a drawing of the average structure of ClMe viewed down the monoclinic **b** axis. Figure 5c shows a drawing of the same

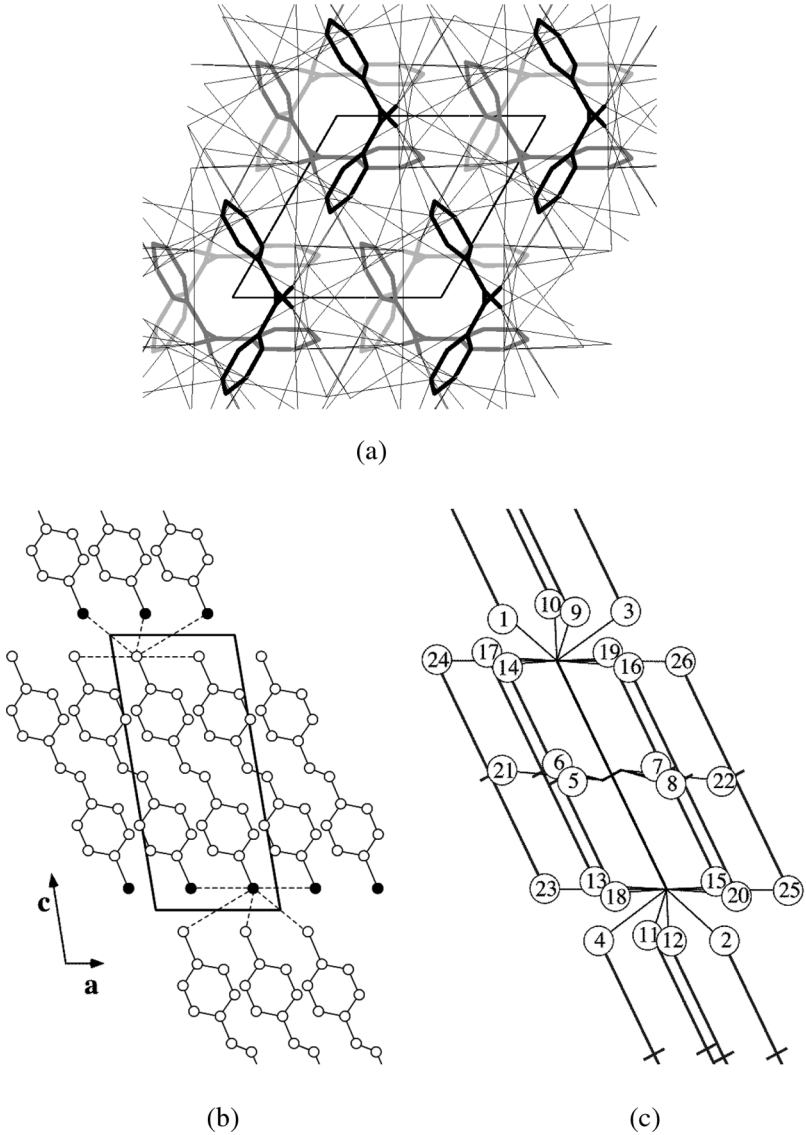

FIGURE 5 (a) Plot of the structure of benzil viewed down **c.** This also shows the 34 contact vectors used to define the effective interactions. (b) Plot of the structure of ClMe viewed down **b**. In this figure all molecules are in the orientation corresponding to $\sigma = +1$, $\rho = +1$. (c) Schematic diagram of the environment of a central molecule of ClMe showing the 26 different vectors along which 'springs' linking the central molecule to its 14 neighbours are placed to represent the effective molecular interactions. In (c) the view is slightly rotated to reveal the neighbouring molecular sites which occur above and below the height of the central molecule.

region of structure in which the molecules have been replaced by the 4-atom *motifs* that were actually used in the simulation. Figure 5c also contains the contact vectors comprising the effective interactions between neighbours. These are referred to by the numbers given in circles at the end of each vector. In this case the central ClMe molecule is in contact with 14 neighbours (7 symmetry-related pairs) and 26 vectors between the 4-atom *motifs* are used to define the effective interactions. These are comprised of 8 different types of vector, as shown in Table 1 and consequently 8 different spring constants $K_{\mathrm{n,m}}$ must be specified. For each of these 8 types of spring, there are in principle 16 different combinations of the orientations of the two molecules in the sites n and m, and consequently 16 different values for the size-effect parameters, $\varepsilon_{n,m}$. Attempting to utilize such a large number of variables with Eq. (3) is simply not feasible and some drastic simplification is necessary. Consequently it was assumed that for vectors involving the ends of the molecules the size-effect parameters were only dependent on the end-to-end flipping (variables $\rho_{i,j,k,l}$) while for vectors involving the middles of the molecules the size-effect was dependent on side-to-side flipping (variables $\sigma_{i,j,k,l}$). In this way each vector required only 4 different values of the size-effect parameters, $\varepsilon_{n,m}$, and since the average vector length must be maintained this meant three independent size-effect parameters per vector or 24 parameters in total.

Before these size-effect parameters could be used the occupancy distribution was first established using Eq. (4) and (5). Again some simplifications were made. First, it was assumed that the SRO could be adequately described using only 3 different near-neighbour types of

TABLE 1 Summary of the Force Constants, Types of Size-Effect Parameters and Occupancy Correlation Constants Used in the MC Simulation of ClMe

Spring constant	Interaction vectors	Determined force constant	Size-effect parameter dependent on	Occupancy correlation constants	Determined occupancy correlation
K_1	1,2	131.8	end-to-end		
K_2	3,4	437.1	end-to-end		
K_3	5,6,7,8	70.0	side-to-side	a_1, b_1	-0.5
K_4	9,10,11,12	72.3	end-to-end	a_2, b_2	$+0.225$
K_5	13,14,15,16	0.0	end-to-end		
K_6	17,18,19,20	272.2	end-to-end		
K_7	21,22	77.8	side-to-side	a_3, b_3	$+0.1$
K_8	23,24,25,26	304.1	end-to-end		
			cross-correlation	c_0	$+0.65$

contact. These are given in column 5 of Table 1. Secondly it was assumed that the same correlations applied for both the side-to-side flipping and the end-to-end flipping. This latter assumption was made because the limited amount of observed data was insufficient to definitively establish correlations for the side-to-side flipping. Making this assumption gave better agreement than an alternative assumption in which random occupancy of the side-to-side variables, $\sigma_{i,j,k,l}$, was assumed. Finally, a single cross-correlation c_0 term in equation (6) was use to directly correlate the $\sigma_{i,j,k,l}$ and $\rho_{i,j,k,l}$ variables at the same site i, j, k, l.

The MC simulation for ClMe therefore was formulated in terms of 8 spring constants, 24 size-effect parameters, 3 short-range correlation parameters and one cross-correlation parameter, making a total of 36 parameters. Subsequently it was found that one of the spring constants refined to zero so that the total number of parameters used in the final model reduced to 32. Even with the quite drastic approximations that were necessary to be made ClMe is computationally much more complex and demanding a system than benzil.

4. LEAST-SQUARES MC REFINEMENT METHOD

We give here a brief description of the automatic refinement method that has been described in detail in ref. [12]. We seek to minimise the sum of squares of the differences between a set of observed diffuse intensities and corresponding calculated intensities. The observed quantities are diffuse scattering intensities measured at individual pixels in various plane sections of the observed diffraction patterns. The corresponding calculated quantities are the suitably scaled values of the intensity obtained at corresponding points in reciprocal space from a MC simulation of a model system having system parameters p_i. These p_i correspond to the system parameters—force constants, size-effect parameters, short-range order correlation interactions, etc.—as described for benzil and ClMe in section 3 above. We minimise the goodness-of-fit, χ^2,

$$\chi^2 = \sum_{h,k,l,m} w_{hklm}(\Delta I)^2, \quad \text{where, } \Delta I = I_{obs} - (b_m + f_m I_{calc}). \qquad (7)$$

Here the summation is over all are non-integral reciprocal points h,k,l corresponding to individual pixels in the m measured sections of data. f_m is a scale and b_m a background correction applied to section m. [Note, f_m and b_m are determined as described in ref. [22] and are not included as variables in the least squares matrix]. ω_{hklm} is a weight which is taken to be equal to $1/I_{obs}$.

Starting from some convenient set of starting parameters the minimisation process entails computing increments Δp_i to be applied to the model parameters. These increments are calculated using:

$$\Delta p_i = \sum_l \mathbf{A}_{il}^{-1} \mathbf{B}_l \tag{8}$$

l is the number of parameters. **A** and **B** involve the differentials of ΔI with respect to each of the variables p_i. **A** is a symmetric matrix and **B** is a vector,

$$A_{ij} = \sum_{hklm} \omega_{hklm} \frac{\partial \Delta I}{\partial p_i} \frac{\partial \Delta I}{\partial p_j} \tag{9}$$

$$B_i = -\sum_{hklm} \omega_{hklm} \, \Delta I_{\text{trial}} \frac{\partial \Delta I}{\partial p_i} \tag{10}$$

The differentials $\partial \Delta I / \partial p_i$ may be computed as follows. If $p = (p_0, p_1, p_2, p_3, \ldots p_i, \ldots p_n)$ is the current set of system parameters, the differential for the i'th parameter can be estimated by performing two complete MC simulation and diffraction pattern calculations, one using the current parameter set, p, and one using an incremented set $p^+ = (p_0, p_1, p_2, p_3, \ldots p_i + \delta_i, \ldots p_n)$, where δ_i is a suitably chosen small increment. The differential is then taken as:

$$\frac{\partial \Delta I}{\partial p_i} = \sum_{hklm} \frac{(\Delta I_p - \Delta I_{p+})}{\delta_i}. \tag{11}$$

In order for these estimates of the differentials to provide a useful signal to the least-squares process the quality of the diffraction pattern calculation must be sufficiently good (smooth, low noise). δ_i must also be sufficiently large that there is significant difference between the two calculations. In Figure 6 we show a diffraction pattern calculated for the ($h0l$) section of benzil using the starting set of parameters together with plots of the difference between this calculation and three similar ones for each of which one of the parameters has been incremented. This figure shows that each parameter alters the calculated diffraction pattern in a clearly distinguishable way.

5. RESULTS

Figure 7 shows observed and calculated diffraction patterns for two sections of the diffraction pattern of benzil and for one section of ClMe.

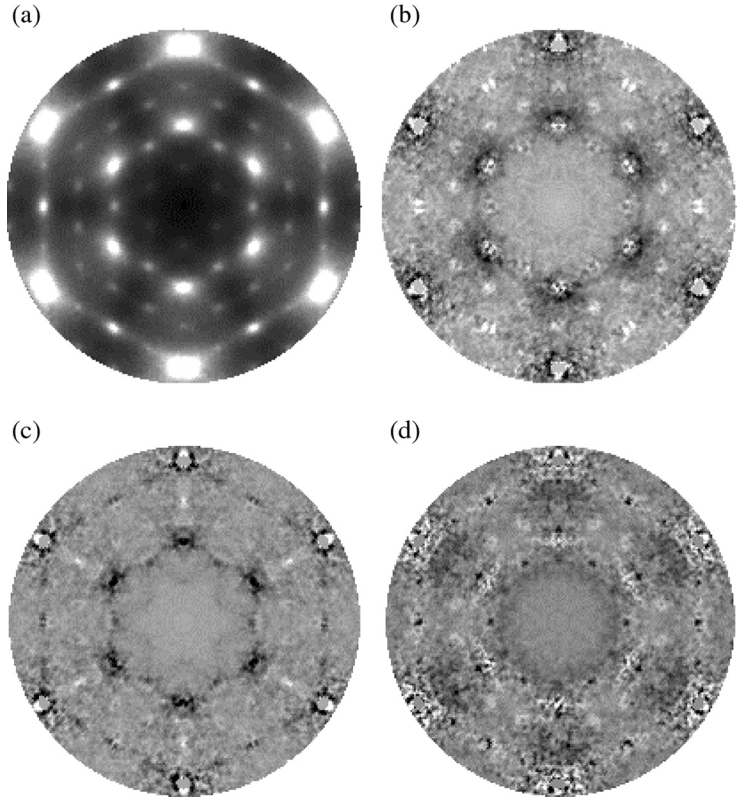

FIGURE 6 Illustration of the calculation of thedifferentials, $\frac{\partial \Delta I}{\partial p_i}$. (a) Plot of the intensity distribution of the (*h0l*) section of benzil calculated from a MC model with all force constants equal. (b), (c) and (d) are plots of the difference in intensity from (a) calculated when three different parameters are incremented. Light and dark show increases or decreases in the calculated intensity relative to (a).

The calculated patterns were obtained from the final MC simulation after fitting of the system parameters as described in Section 3. Values for the force constant parameters are given in Table 1. The final agreement factor, $R = (\sum \omega(\Delta I)^2 / \sum \omega I_{obs}^2)^{1/2}$, was 14.5% for benzil and 32.8% for ClMe. The agreement for benzil is thus truly quantitative and is close to being comparable to the agreement levels obtained for Bragg intensities (note that R here relates to intensity rather than structure factor). One particularly significant result of the refinement is that the R value obtained when the torsional force constants for the ϕ_1, ϕ_2, ϕ_3 angles was set to zero was $\sim$18%. That is, the analysis is

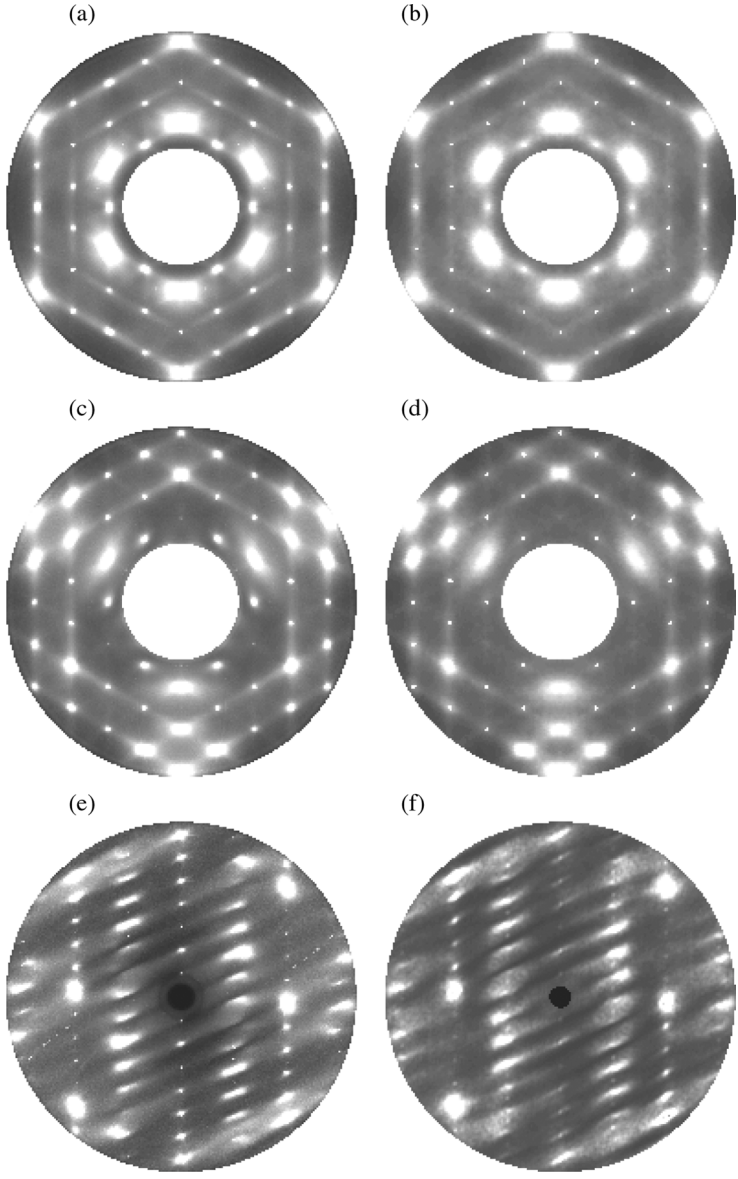

FIGURE 7 Final observed and calculated diffraction patterns for benzil and ClMe. (a) Benzil observed (*hk0*). (b) Benzil calculated (*hk0*). (c) Benzil observed (*hk2*). (d) Benzil calculated (*hk2*). (e) ClMe (*h0l*) observed. (f) ClMe (*h0l*) calculated.

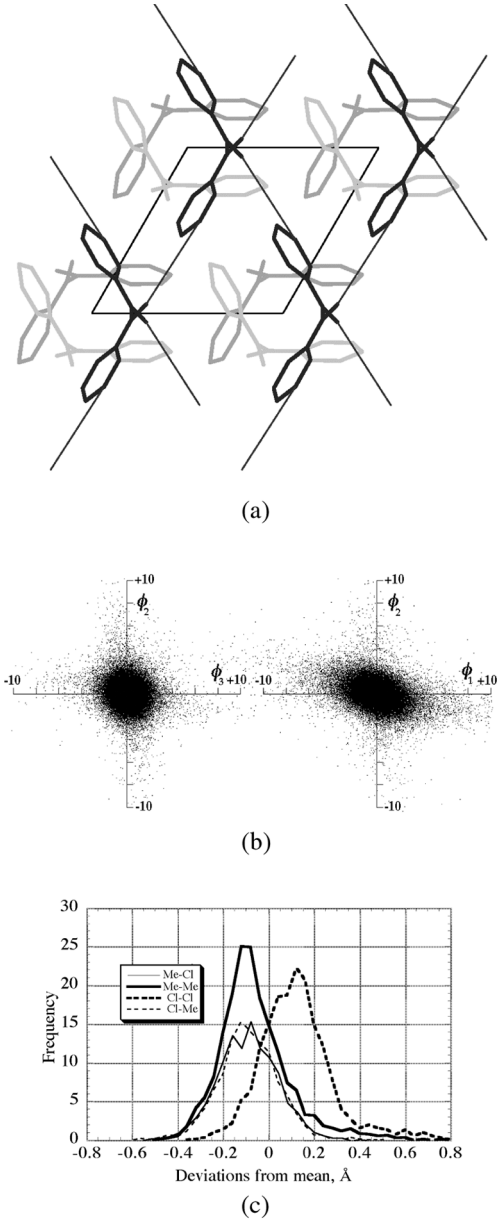

FIGURE 8 (a) Plot showing the 2D network formed in the benzil simulation by intermolecular springs having the strongest force constant. (b) Plot the distribution of the torsion angles ϕ_2 vs. ϕ_3 and ϕ_1 vs. ϕ_2 away from their mean values for all of the molecules in the benzil simulation. (c) Plot of the distribution of the length of vector 3 away from its mean in the ClMe simulation as a function of the vector type (Me-Me, Cl-Me, Me-Cl, Cl-Cl).

clearly able to distinguish that these torsional angles do not rotate freely. The agreement for ClMe is not nearly so good and this is undoubtedly a reflection of the numerous approximations that had to be made for this much more complex problem. Nevertheless it is clear from a visual comparison of the observed and calculated patterns that most of the different diffuse features in the pattern have been modeled quite well and that the analysis has satisfactorily determined the key features of the problem. As available computational resources improve it is likely that some of the approximations that were made could be lifted and this should allow a better fit to be obtained.

Exploring the final MC simulation distributions reveals some interesting features of the two models. In the case of benzil the analysis shows quite clearly that the diffuse lines that feature so prominently in the observed diffraction patterns are due to strong longitudinal displacement correlations. By *longitudinal correlation* we mean that the direction of displacement and the direction of correlation are the same. These are transmitted from molecule to molecule via a network of contacts that correspond to the strongest force constant (see Fig. 8a). It seems likely that the real molecular basis for this is hydrogen bonding between an O atom on one molecule and the *para* H atom of the phenyl ring of a neighbouring molecule. These interactions form a flexible 2D network linking all the molecules in layers normal to **c**. The flexing of this network, which gives rise to the correlated displacements, involves the coupling of the internal torsion angle, ϕ_1, with the molecular translations.

It is also interesting to plot the distribution of the torsion angles ϕ_2 vs. ϕ_3 and ϕ_1 vs. ϕ_2 for all of the molecules present in the final simulation (see Fig. 8b). Since the model contains no direct forces correlating the angles, any departure from a circularly symmetric distribution is indicative of the fact that the external inter-molecular forces act on the molecules to produce correlation between the angles. Figure 8b shows that there is significant correlation between ϕ_1 and ϕ_2 (and also ϕ_1 and ϕ_3) but very little between ϕ_2 and ϕ_3.

For the ClMe analysis the most significant finding relates to the size-effect parameters. In particular it is found that the average distances in the simulation results for the vector 3 (and its symmetry equivalent vector 4) show a substantial size-effect. That is, this vector is substantially different in length depending on the mutual orientation of the central molecule and the neighbour connected by vector 3. In Figure 8c we show a plot of the distribution of this vector distance observed over all unit cells in the simulation. It is seen from this plot that when the vector corresponds to a contact between the Cl-end of both molecules the distance is about 0.2 to 0.3 Å greater than for other

combinations (Cl-Me, Me-Cl and Me-Me). It is this 'size-effect' that produces the strong asymmetry that is observed in some of the diffuse peaks seen in the observed data (Fig. 7e).

CONCLUSION

We have shown in this paper that the measurement of diffuse scattering data over large volumes of reciprocal space is now relatively routine and this opens up the possibility of analysing the local atomic and molecular structure of crystals in a level of detail not possible via conventional crystallography. In addition we have described the development of a general method by which diffuse scattering data can be analysed. This involves the setting up of a computer model of the structure and using MC simulation to generate realisations from which diffraction patterns may be calculated and compared to the observed data. The MC simulation is set up in terms of a parameters describing basic intermolecular interactions and any disorder effects that may be present and these parameters are adjusted iteratively to provide the best fit of the MC model to the observed data. This method is very computer-intensive and is only just becoming a viable possibility with current computational resources. The method has been illustrated using two contrasting organic molecular crystal examples. In the case of benzil the diffuse scattering is purely thermal in origin and a MC model involving only 13 parameters was able to give a quantitative fit to the data. ClMe on the other hand is very disordered with each molecular site being occupied by the molecule in one of four different basic orientations and considerable local relaxation of these basic positions and orientations is present. In this case it was necessary to make a number of quite drastic simplifying assumptions for the analysis to be viable and consequently the resulting fit to the data was not quite so quantitative. Despite this the model obtained reproduced all the essential features of the diffraction pattern and gave much valuable insight into what was occurring in the crystal. As computational resources increase it should be possible to dispense with some of the simplifications that were made and refine the model to give a more quantitative fit.

As the methodology described here further develops and improves and the computation power available continues to increase we fully expect that the analysis of diffuse scattering will become increasingly routine for a wide variety of materials. This promises a bright future where structural information available to researchers will no longer be confined to the average one-body information contained in the Bragg peaks.

REFERENCES

[1] Hayakawa, M. & Cohen, J. B. (1975). Equations for diffuse scattering from materials with multiple sublattices. *Acta Cryst.*, *A31*, 635–645.

[2] Tibballs, J. E. (1975). The separation of displacement and substitutional disorder scattering: a correction for structure-factor ratio variation. *J. Appl. Cryst.*, *8*, 111–114.

[3] Butler, B. D. & Welberry, T. R. (1993). Interpretation of displacement-caused diffuse scattering using the Taylor expansion. *Acta Cryst.*, *A49*, 736–743.

[4] Welberry, T. R. & Butler, B. D. (1994). Interpretation of diffuse X-ray scattering via models of disorder. *J. Appl. Cryst.*, *27*, 205–231.

[5] Mayo, S. C., Proffen, T., Bown, M., & Welberry, T. R. (1999). Diffuse scattering and Monte Carlo simulations of cyclohexane-perhydrotriphenylene (PHTP) inclusion compounds, $C_6H_{12}/C_{18}H_{30}$. *J. Appl. Cryst.*, *32*, 464–471.

[6] Welberry, T. R., Hua, G. L., & Withers, R. L. (1989). An optical transform and Monte Carlo study of the disorder in β-cristobalite SiO_2. *J. Appl. Cryst.*, *22*, 87–95.

[7] Welberry, T. R. & Mayo, S. C. (1996). Diffuse X-ray Scattering and Monte-Carlo Study of Guest-Host Interactions in Urea Inclusion Compounds. *J. Appl. Cryst.*, *29*, 353–364.

[8] Welberry, T. R. & Glazer, A. M. (1994). Diffuse X-ray scattering in potassium lithium sulfate, $KLiSO_4$. *J. Appl. Cryst.*, *27*, 733–741.

[9] Welberry, T. R. & Christy, A. G. (1997). Defect distribution and the diffuse X-ray diffraction pattern of wüstite, $Fe_{1-x}O$. *Phys. Chem. Minerals*., *24*, 24–38.

[10] Welberry, T. R., Butler, B. D., Thompson, J. G., & Withers, R. L. (1993). A 3D model for the Diffuse Scattering in Cubic Stabilised Zirconias. *J. Solid State Chem.*, *106*, 461–475.

[11] Welberry, T. R. & Withers, R. L. (1990). An Optical transform and Monte Carlo Study of the Diffuse X-ray Scattering in Mullite, $Al_2(A_{l2+2x}Si_{2-2x})O_{10-x}$. *Phys. Chem. Minerals*., *17*, 24–38.

[12] Welberry, T. R., Proffen, T., Bown, M. (1998). Analysis of Single-Crystal Diffuse X-ray Scattering via Automatic Refinement of a Monte Carlo Model. *Acta Cryst.*, *A54*, 661–674.

[13] Welberry, T. R., Goossens, D. J., Edwards, A. J., & David, W. I. F. (2001). Diffuse X-ray scattering from benzil, $C_{14}H_{10}O_2$: analysis via automatic refinement of a Monte Carlo model. *Acta Cryst.*, *A57*, 101–109.

[14] Welberry, T. R. (2000). Diffuse X-ray scattering and disorder in *p*-methyl-*N*-(*p*-chlorobenzylidene)aniline, $C_{14}H_{12}ClN$ (ClMe): analysis via automatic refinement of a Monte Carlo model. *Acta Cryst.*, *A56*, 348–358.

[15] Osborn, J. C. & Welberry, T. R. (1990). A position-sensitive detector system for the measurement of diffuse X-ray scattering. *J. Appl. Cryst.*, *23*, 476–484.

[16] Welberry, T. R., Goossens, D. J., Haeffner, D. R., Lee, P. L., & Almer, J (2003). High-energy diffuse scattering on the 1-ID beamline at the Advanced Photon Source. *J. Synchrotron Rad.*, *10*, 284–286.

[17] Weber, T., Estermann, M. A., & Bürgi, H.-B. (2001). Structural complexity of a polar perhydro tri-phenylene inclusion compound brought to light by synchrotron radiation. *Acta Cryst.*, *B57*, 579–590.

[18] Campbell, B. J., Welberry, T. R., Broach, R. W., Hong, H., & Cheetham, A. K. (2003). Elucidation of zeolite microstructure by synchrotron X-ray diffuse scattering. *J. Appl. Cryst.*, in press.

[19] Keen, D. A. & Wilson, C. C. (1996). Single Crystal Diffraction at ISIS – User Guide for the SXD Instrument. RAL Technical Report. RAL-TR-96–083.

[20] Welberry, T. R., Goossens, D. J., David, W. I. F., Gutmann, M. J., Bull, M. J., & Heerdegen, A. P. (2003). Diffuse neutron scattering in benzil, $C_{14}D_{10}O_2$, using the time-of-flight Laue technique. *J. Appl. Cryst.*, *36*, 1440–1447.
[21] Beyer, T., Day, G. M., & Price, S. L. (2001). The prediction, morphology and mechanical properties of the polymorphs of paracetamol. *J. Am. Chem. Soc.*, *123*, 5086–5094.
[22] Proffen, T. & Welberry, T. R. (1997). Analysis of Diffuse Scattering via the Reverse Monte Carlo Technique: a Systematic Investigation. *Acta Cryst.*, *A53*, 202–216.